AD-A134 274 WHISTLER MODE TURBULENCE GENERATED BY ELECTRON BEAMS IN EARTH'S BOW SHOCK.. (U) IOWA UNIV IOWA CITY DEPT OF PHYSICS AND ASTRONOMY R L TOKAR ET AL. MAY 83 1/1

UNCLASSIFIED U. OF IOWA-83-17 N00014-76-C-0016 F/G 4/1 NL

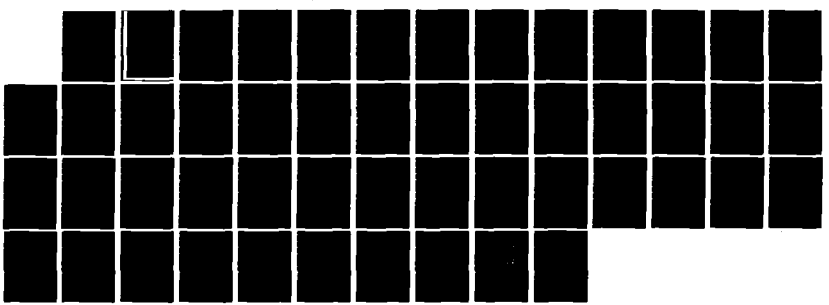

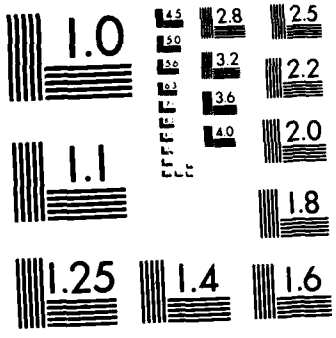

Whistler Mode Turbulence Generated by Electron Beams in Earth's Bow Shock

by

R. L. Tokar[1], D. A. Gurnett[1], and W. C. Feldman[2]

Department of Physics and Astronomy
THE UNIVERSITY OF IOWA
Iowa City, Iowa 52242

U. of Iowa 83-17

Whistler Mode Turbulence Generated by Electron Beams in Earth's Bow Shock

by

R. L. Tokar[1], D. A. Gurnett[1], and W. C. Feldman[2]

May 1983

[1] Department of Physics and Astronomy
The University of Iowa
Iowa City, IA 52242

[2] Los Alamos Scientific Laboratory
Los Alamos, NM 87545

To appear in J. Geophys. Res.

This research was supported by NASA through Grants NGL-16-001-002 and NGL-16-001-043 from NASA Headquarters and Contract NAS5-26819 from Goddard Space Flight Center and by the Office of Naval Research through Contract N00014-76-C-0016.

UNCLASSIFIED

SECURITY CLASSIFICATION OF THIS PAGE (When Data Entered)

REPORT DOCUMENTATION PAGE		READ INSTRUCTIONS BEFORE COMPLETING FORM
1. REPORT NUMBER: U. of Iowa 83-17	2. GOVT ACCESSION NO.: AD-A134274	3. RECIPIENT'S CATALOG NUMBER:
4. TITLE (and Subtitle): WHISTLER MODE TURBULENCE GENERATED BY ELECTRON BEAMS IN EARTH'S BOW SHOCK		5. TYPE OF REPORT & PERIOD COVERED: Progress, May, 1983
		6. PERFORMING ORG. REPORT NUMBER:
7. AUTHOR(s): R. L. TOKAR, D. A. GURNETT, and W. C. FELDMAN		8. CONTRACT OR GRANT NUMBER(s): N00014-76-C-0016
9. PERFORMING ORGANIZATION NAME AND ADDRESS: Department of Physics and Astronomy, The University of Iowa, Iowa City, IA 52242		10. PROGRAM ELEMENT, PROJECT, TASK AREA & WORK UNIT NUMBERS:
11. CONTROLLING OFFICE NAME AND ADDRESS: Office of Naval Research, Electronics Program Office, Arlington, VA 22217		12. REPORT DATE: May, 1983
		13. NUMBER OF PAGES: 47
14. MONITORING AGENCY NAME & ADDRESS(if different from Controlling Office)		15. SECURITY CLASS. (of this report): UNCLASSIFIED
		15a. DECLASSIFICATION/DOWNGRADING SCHEDULE:

16. DISTRIBUTION STATEMENT (of this Report)

Approved for public release; distribution is unlimited.

17. DISTRIBUTION STATEMENT (of the abstract entered in Block 20, if different from Report)

18. SUPPLEMENTARY NOTES

To be published in J. Geophys. Res.

19. KEY WORDS (Continue on reverse side if necessary and identify by block number)

Bow shock, Whistler Mode Waves

20. ABSTRACT (Continue on reverse side if necessary and identify by block number)

(See page following)

DD FORM 1 JAN 73 1473 EDITION OF 1 NOV 65 IS OBSOLETE
S/N 0102-LF-014-6601

UNCLASSIFIED

SECURITY CLASSIFICATION OF THIS PAGE (When Data Entered)

ABSTRACT

In this study, the Landau and cyclotron growth rates of whistler mode waves in Earth's bow shock are calculated using electron distribution functions obtained with the fast plasma experiment on ISEE 2. Three electron distribution functions measured within the transition region of the shock are analyzed. An important feature of these electron distribution functions is the presence of a field-aligned beam with a $T_\perp > T_\parallel$ anisotropy. The beam velocity vector is directed toward the magnetosheath. The calculations show that the electron distribution functions spontaneously generate whistler mode waves with plasma rest frame frequencies between about .1 and 100 Hz. The wave normal angles of the generated whistlers range from 0° to the resonance cone angle. Electromagnetic Landau resonance and/or cyclotron resonance contribute to wave growth over the range of velocity distributions observed. The waves that are generated by the normal cyclotron resonance have wave vectors directed toward the solar wind while those that are generated by the Landau and the anomalous cyclotron resonances have wave vectors directed toward the magnetosheath. The predictions of the study are in qualitative agreement with observations of whistler mode waves near Earth's bow shock.

I. INTRODUCTION

Although shock waves in collisionless plasmas have been studied for more than two decades, the physics of collisionless shocks is still not well understood. Much of the current theoretical effort is aimed at formulating models that self-consistently describe the observed shock structures and the shock dissipation mechanisms. In a collisionless shock wave the upstream unshocked plasma is transformed into the downstream shocked plasma within a spatial length that is smaller than the mean free paths of the plasma particles. The region separating the upstream and downstream plasmas within which the dissipation occurs is called the transition region. Observations of fluctuating electric and magnetic fields associated with shocks in the laboratory and in interplanetary space indicate that plasma wave turbulence plays an important role in electron and ion heating at the shock. For information and additional references on the subject of both natural and laboratory shock waves, the interested reader can refer to Tidman and Krall [1971], Biskamp [1973], Galeev [1976], Formisano [1977], and Greenstadt and Fredericks [1979].

Earth's bow shock, the shock wave formed by the interaction of the solar wind with Earth's magnetic field, provides an excellent laboratory for the study of collisionless shock waves. The characteristics of the bow shock are highly variable because the parameters that

characterize the upstream solar wind vary over a broad range. In addition, because spacecraft instruments have dimensions smaller than characteristic shock scale lengths, the shock fine structure can be studied in detail if high time resolution instrumentation is used or if the spacecraft is moving slowly with respect to the shock.

Among the experiments on board the ISEE 1 and 2 satellites are a fast plasma experiment [Bame et al., 1978] and a plasma wave experiment [Gurnett et al., 1978]. The fast plasma experiment is specifically designed to measure distribution functions in one dimension in approximately 100 milliseconds and distribution functions in two dimensions in one spin period (3 seconds). In particular, the time resolution of the fast plasma experiment is sufficient to allow the measurement of distinctive features of electron distribution functions within the shock transition region with negligible aliasing of time. An important new feature of the electron distribution functions measured by the fast plasma experiment within the shock transition region is a field-aligned beam moving toward the magnetosheath [Feldman et al., 1982; 1983]. The beam is observed for both quasi-parallel and quasi-perpendicular turbulent shocks. Quasi-parallel and quasi-perpendicular refer to the angle between the shock normal and the ambient magnetic field, θ_{Bn}. For a quasi-parallel shock, θ_{Bn} is greater than 0° but less than about 45° while for a quasi-perpendicular shock θ_{Bn} is greater than about 45° but less than 90°.

The plasma wave experiment observes many types of plasma turbulence in association with Earth's bow shock. This turbulence is similar to the plasma waves observed near the bow shock by previous

instrumentation [Fredericks et al., 1968; Rodriguez and Gurnett, 1975]. Among the different types of electrostatic and electromagnetic waves observed is whistler mode turbulence. Whistler mode waves are electromagnetic waves that propagate at frequencies below either the electron gyrofrequency, ω_g, or the electron plasma frequency, ω_p. In the solar wind and bow shock regions, ω_g is always much less than ω_p. Typically, the whistler mode noise is most intense within the shock transition region and is observed to extend short distances into the upstream solar wind and much longer distances into the downstream magnetosheath.

The purpose of this study is to demonstrate that the electron beams measured by the ISEE 2 fast plasma experiment in the transition region of the bow shock can generate whistler mode instabilities. The generation mechanisms are identified and the subsequent propagation of the whistler mode waves are discussed.

In addition to data obtained with the fast plasma experiment and the plasma wave experiment, the study also makes use of data obtained with the ISEE 1 and 2 magnetic field experiment [Russell, 1978].

II. TRANSITION REGION ELECTRON DISTRIBUTION FUNCTIONS

The electron distribution functions analyzed in this study were measured by the fast plasma experiment within the transition region of Earth's bow shock. In many instances, it is possible to fit the data obtained by the fast plasma experiment to simple analytic functions. Because the measurement of and fitting procedure for these electron distribution functions is described in detail in the recent reports of Feldman et al. [1982, 1983], only a brief summary will be given here.

In Figure 1, slices of electron distribution functions measured along the direction of the magnetic field on December 13, 1977, by the ISEE 2 fast plasma experiment are shown. This figure is reproduced from Feldman et al. [1982]. The figure depicts parallel slices in the solar wind (SW), the shock transition region, and the magnetosheath (MS). Data for the full two-dimensional electron distribution function obtained with the fast plasma experiment suggests that the solar wind electron distribution function is a nearly isotropic Maxwellian at this time and that the magnetosheath electron distribution function is a nearly isotropic modified Lorentzian at this time. As the satellite enters the shock transition region, field-aligned electron beams are observed. The beams are moving toward the magnetosheath and the beam velocity increases with increasing shock penetration. This figure supports the fact that the electron distribution functions measured in

the shock transition region have both a flat-topped component and a beam component.

The analytic representation of the electron distribution function in the plasma rest frame, $F(v_\perp, v_\parallel)$, is constructed from two measurements of the electron distribution function in planes parallel ($v_\parallel$) and perpendicular ($v_\perp$) to the ambient magnetic field separated in time by about 0.75 sec. Measurements of the electron distribution function in planes other than those parallel and perpendicular to the magnetic field confirm that the fits to these two data sets yield, for the purposes of this study, a sufficiently accurate representation of $F(v_\perp, v_\parallel)$. The simple analytic function used to fit the data is a sum of a convected Maxwellian and a modified Lorentzian. The convected Maxwellian models the electron beam and the modified Lorentzian models the flat-topped component of the electron distribution function. These models provide excellent fits to both the parallel and the perpendicular slices of the distribution function.

Specifically, $F(v_\perp, v_\parallel)$ is given by

$$F(v_\perp, v_\parallel) = F_1 + F_2$$

where

$$F_1 = \frac{C_1}{\left(1 + \left(\frac{(v_\parallel - v_1)^2 + v_\perp^2}{v_2^2}\right)^R\right)^{P/R}}$$

is the modified Lorentzian and

$$F_2 = C_2 \exp\left(\frac{-m(v_\parallel - v_3)^2}{2\kappa T_\parallel}\right)\exp\left(\frac{-m\, v_\perp^2}{2\kappa T_\perp}\right)$$

is the convected Maxwellian. In these equations, P and R are real numbers, $T_\perp$ and $T_\parallel$ are perpendicular and parallel temperatures, m is the electron mass, κ is Boltzman's constant, and C_1, C_2, v_1, v_2 and v_3 are constants.

It should be noted that for the electron distribution functions analyzed in this study, the direction of positive $v_\parallel$, be it parallel or anti-parallel to the magnetic field, is determined by the bow shock geometry at the observation time. The positive $v_\parallel$ direction is defined to be such that $\hat{v}_\parallel \cdot \hat{n}$ is positive, where $\hat{v}_\parallel$ is a unit vector in the positive $v_\parallel$ direction and $\hat{n}$ is a unit vector in the direction of the shock normal and toward the solar wind. Consequently, because the beam velocity vectors are always directed toward the magnetosheath, the convection speed, v_3, is always negative.

The magnitude of the beam convection speed increases with increasing shock penetration. This variation is consistent with the interpretation that the beams represent solar wind electrons that are accelerated by a macroscopic electric field within the shock transition region. The parallel temperature of the beam, $T_\parallel$, is obtained from the fit to the fast plasma experiment data. However, in many cases the corresponding perpendicular beam temperature, $T_\perp$, changes significantly

during the time it takes for the detector to rotate from the parallel to the perpendicular orientations. Consequently, $T_\perp$ is estimated assuming that the first adiabatic invariant of the electrons is conserved as the electrons move from the solar wind into the shock. When the relative motion between the spacecraft and the bow shock is sufficiently slow so that $T_\perp$ can be obtained, the calculated and measured perpendicular beam temperatures are in good agreement.

In this study, three electron distribution functions measured by the ISEE 2 fast plasma experiment within the transition region of Earth's bow shock are analyzed. Of the three, two were measured on December 13, 1977, and one was measured on October 15, 1978. The two electron distribution functions obtained in the transition region on December 13, 1977, correspond closely to the distributions measured at 17:34:55.8 and 17:34:58.6 that are depicted in Figure 1. The October 15, 1978, electron distribution function is included in this study because the magnitude of the convection speed of the Maxwellian modelling the electron beam is particularly small, which leads to somewhat different instability conditions than for the December 13 cases.

In Figure 2, contour plots of the best-fitting analytic models for the three electron distribution functions analyzed in this study are shown. Plotted are contours of constant $\log_{10} F(v_\perp, v_\parallel)$ spanning one order of magnitude of F. The convected Maxwellians with $T_\perp > T_\parallel$ anisotropies that model the electron beams are clearly visible as is the flat-topped feature of the modified Lorentzians. In Table 1, the constants used to specify these three electron distribution functions

are given. In Table 2, the bow shock parameters at the three observation times are summarized. For both shock crossings, the bow shock classification is turbulent.

III. METHOD OF CALCULATING THE GROWTH RATE

To calculate the growth rate of whistler mode waves, the results obtained by Kennel and Wong [1967] using the linearized Vlasov and Maxwell equations are employed. The expression used is equivalent to the results given by Kennel [1966]. If Landau and first order cyclotron resonance terms are included and ion motion is neglected, the growth rate, ω_i, is given by

$$\omega_i = |\omega_r| \text{sign}\left(\frac{\omega_r}{k_\parallel}\right) \frac{\omega_p^2}{\omega_r^2} \frac{\pi}{16} \int_0^\infty v_\perp^2 (I_{-1} + I_o + I_1) dv_\perp \tag{1}$$

where

$$I_m = \left. \frac{(\varepsilon_L J_{m-1}(x) + \varepsilon_R J_{m+1}(x) - \sqrt{2}\left(\frac{v_\parallel}{v_\perp}\right)\varepsilon_\parallel J_m(x))^2 \left(v_\perp \frac{\partial F}{\partial v_\parallel} - \frac{m\omega_g}{k_\parallel} \frac{\partial F}{\partial v_\perp}\right)}{W} \right|_{v_\parallel = \frac{\omega_r + m\omega_g}{k_\parallel}}$$

and W, the total wave energy, is given by

$$W(\vec{k},\omega) = \frac{1}{16\pi} \left[\vec{B}^*(\vec{k},\omega) \cdot \vec{B}(\vec{k},\omega) + \vec{E}^*(\vec{k},\omega) \cdot \left(\frac{\partial}{\partial\omega} \omega \overleftrightarrow{K}^h\right) \cdot \vec{E}(\vec{k},\omega)\right]$$

In these equations, F is the electron distribution function normalized to unity, ω_r is the real frequency of the wave, k is the wave number, ε_L, ε_R, and $\varepsilon_\parallel$ are the left-hand, right-hand, and parallel electric field polarization vectors of the wave, $\bar{\bar{K}}^h$ is the Hermitian part of the dielectric tensor, ω_g is the absolute value of the electron gyrofrequency, and x is $\frac{k_\perp v_\perp}{\omega_g}$. The Landau contribution to the growth rate is the m = 0 term and the normal and anomalous cyclotron resonance contributions are given by the m = -1 and the m = +1 terms. A positive growth rate indicates exponential growth and a negative growth rate indicates exponential damping.

In order to employ Equation 1 to calculate growth rates for whistler mode waves, the real part of the whistler mode dispersion relation must be solved for ω_r as a function of k. For simplicity, this study assumes that the real part of the whistler mode dispersion relation is that of a cold plasma. When the wave phase velocity is much greater than the electron thermal speed, hot plasma effects on dispersion for the whistler mode are small (e.g., see Leimohn [1962]). However, in the work reported here the wave phase velocities are often comparable to the electron thermal velocities. To investigate the error introduced by this simplifying assumption, the numerical code of Forslund [1979], which solves the fully electromagnetic linear dispersion relation, has been utilized to determine the real frequency, ω_r, for a given wave number, k [S. P. Gary, private communication]. For parameters typical of this study, the results indicate that for a given wave number and for wave normal angles $\theta \lesssim 45°$, where the wave normal

angle is the angle between the wave vector and the magnetic field, the real frequency for a cold plasma and the real frequency obtained using the code of Forslund differ by not more than 30 percent. If k is held constant and ω_r is allowed to vary by 30 percent, the computations show that the change in the growth rate calculated using Equation 1 is, for the majority of unstable wave numbers, small. As the wave normal angle approaches the resonance cone angle, $\theta_{Res} \approx \cos^{-1}(\frac{\omega_r}{\omega_g})$, the index of refraction becomes infinite and the wave becomes predominantly electrostatic. For wave normal angles near the resonance cone angle, the difference between the real frequency for a cold plasma and the real frequency obtained using the code of Forslund for a given k is larger than it is for small wave normal angles. Consequently, it should be noted that while the primary results of this study are not affected by the simplifying assumption used in calculating the growth rate, the calculated growth rates for wave normal angles near θ_{Res} are not accurate.

IV. GROWTH RATE CALCULATIONS AND GENERATION MECHANISMS

Growth rates for whistler mode waves have been calculated using Equation 1 and the electron distribution functions depicted in Figure 2. The results indicate that these electron distribution functions are unstable to whistler mode waves. In this section, the growth mechanisms that generate the whistler mode waves are discussed.

From Equation 1 it is observed that the total growth rate is a sum of three terms: the two cyclotron resonance contributions and the Landau resonance contribution. The sign of the growth rate is positive if the sum of the three contributions is positive. The signs of the $m = -1$, 0, and +1 contributions are positive or negative depending on whether or not the following quantity is positive or negative:

$$\text{sign}\left(\frac{\omega_r}{k_\parallel}\right) \int_0^\infty \left(v_\perp \frac{\partial F}{\partial v_\parallel} - \frac{m\omega_g}{k_\parallel} \frac{\partial F}{\partial v_\perp}\right) \Bigg|_{v_\parallel = \frac{\omega_r + m\omega_g}{k_\parallel}} v_\perp^2 dv_\perp \qquad (2)$$

which can be rewritten in the form

$$\text{sign}\left(\frac{\omega_r}{k_\parallel}\right) \int_0^\infty \left(v_\perp \frac{\partial F}{\partial v_\parallel} + \left(\frac{\omega_r}{k_\parallel} - v_\parallel\right)\frac{\partial F}{\partial v_\perp}\right)\Bigg|_{v_\parallel = \frac{\omega_r + m\omega_g}{k_\parallel}} v_\perp^2 dv_\perp \quad . \tag{3}$$

Integrating the second term in Equation 3 by parts and introducing the electron pitch angle, α, where α is measured from the positive $v_\parallel$ axis, Equation 3 can be rewritten as

$$\text{sign}\left(\frac{\omega_r}{k_\parallel}\right) \left[-\frac{2\omega_r}{k_\parallel} \int_0^\infty F v_\perp dv_\perp - \int_0^\infty \frac{\partial F}{\partial \alpha} v_\perp^2 dv_\perp\right]\Bigg|_{v_\parallel = \frac{\omega_r + m\omega_g}{k_\parallel}} \quad . \tag{4}$$

The whistler mode waves generated in the transition region by the electron distribution functions shown in Figure 2 fall naturally into two categories: waves with wave vectors predominantly in the opposite direction of the beam velocity and waves with wave vectors predominantly in the direction of the beam velocity. For waves propagating in the direction opposite to the beam, i.e., toward the solar wind, $k_\parallel$ is positive and the growth mechanism is the normal $m = -1$ cyclotron resonance. All three electron distribution functions shown in Figure 2 generate whistler mode waves via the $m = -1$ cyclotron resonance. For waves propagating in the direction of the beam, i.e., toward the magnetosheath, $k_\parallel$ is negative and the growth mechanisms are the $m = 0$ Landau and the anomalous $m = +1$ cyclotron resonance. Of the three electron distribution functions shown in Figure 2, only the

distribution function measured on October 15, 1978, generates whistler mode waves propagating in the direction of the beam. In the following subsections, the cases $k_{\parallel} > 0$ and $k_{\parallel} < 0$ are examined.

A. Wave Vectors Directed Toward the Solar Wind: Generation Via the m = -1 Resonance

To investigate the generation of whistler mode waves by the normal m = -1 cyclotron resonance contribution to the growth rate, consider Equations 2 through 4 when m = -1. Because the beams depicted in Figure 2 are moving in the direction of the magnetosheath, the parallel component of the wave vector must be positive for interactions via the m = -1 cyclotron resonance. For the distribution functions shown in Figure 2, the second term in Equation 2 is negative. Therefore, in order for Equation 2 to be positive, $v_{\perp}^{3} \frac{\partial F}{\partial v_{\parallel}}$ evaluated at the m = -1 cyclotron resonance velocity, $v_{\parallel} = \frac{\omega_r - \omega_g}{k_{\parallel}}$, and integrated over all $v_{\perp}$ must be sufficiently positive to overcome the negative term. Equivalently, Equation 4 expresses the result that a region of sufficiently large anisotropy, $\frac{\partial F}{\partial \alpha} < 0$, along the m = -1 cyclotron resonance velocity must exist if the growth rate is to be positive.

From these facts it is expected that the electron distribution functions shown in Figure 2 will generate whistler mode waves if the cyclotron resonance velocity has a larger magnitude than the magnitude of the convection speed of the Maxwellian modelling the electron beam, $|v_3|$. In this region of the electron distribution functions shown in Figure 2, $\frac{\partial F}{\partial v_{\parallel}}$ is positive and $\frac{\partial F}{\partial \alpha}$ is negative.

The left column of Figure 3 shows representative growth rates obtained using the electron distribution function measured within the shock transition region at 1734:55.7 on December 13, 1977. At this time, $\frac{\omega_g}{2\pi}$ is about 315 Hz and $\frac{\omega_p}{2\pi}$ is about 20 kHz. Plotted are the ratios of total growth rate, ω_I, to real frequency, ω_r, as a function of the wave normal angle. The growth rates for the two frequencies $\omega_r/2\pi$ = 110, and 120 Hz are given. This figure depicts whistler mode waves with positive growth rates. The absence of a plotted growth rate indicates damping. For the frequencies shown here, both the m = +1 cyclotron resonance contribution to ω_I and the m = 0 Landau resonance contribution to ω_I are negative and small compared to the positive contribution of the m = -1 cyclotron resonance. The left column of Figure 3 indicates that as the frequency is increased the range of unstable wave normal angles decreases while the centroids of these angles, which range from 0 to about 80 degrees, increase. This trend can be understood from a plot of the m = -1 cyclotron resonance velocity.

The right column of Figure 3 shows the m = -1 cyclotron resonance velocity as a function of wave normal angle for the two frequencies $\frac{\omega_r}{2\pi}$ = 110 and 120 Hz. For the electron distribution function measured at 1734:55.7 on December 13, 1977, the Maxwellian modelling the electron beam is convected into the shock at a speed of about 3255 km/s. It is expected that the resonance velocity must have a larger negative value than -3255 km/s if instability is to occur as only then will $\partial F/\partial \alpha$ be

sufficiently negative (or $\partial F/\partial v_\parallel$ sufficiently positive) along the integration path. This point is illustrated in Figure 4 where the resonance velocity range giving rise to instability for the case $\frac{\omega_r}{2\pi}$ = 110 Hz, as obtained from Figure 3, is overlayed on a contour plot of the electron distribution function measured at 1734:55.7 on December 13, 1977. The resonance velocity lies in a region of positive $\frac{\partial F}{\partial v_\parallel}$ and large anisotropy, $\frac{\partial F}{\partial \alpha} < 0$.

B. Wave Vectors Directed Toward the Magnetosheath: Generation Via the m = 0 and +1 Resonances

To investigate the generation of whistler mode waves by the m = 0 Landau and the m = +1 anomalous cyclotron resonances, Equations 2 through 4 are again examined. Because the convection speeds for the electron beams shown in Figure 2 are negative, for the generation of whistler mode waves via the m = 0 and the m = +1 interactions $k_\parallel$ is negative, corresponding to wave vectors directed toward the magnetosheath.

From Equation 2 it is seen that in order for the m = 0 Landau contribution to ω_i to be positive, $-v_\perp^3 \frac{\partial F}{\partial v_\parallel}$ evaluated at the Landau resonance velocity, $v_\parallel = \frac{\omega_r}{k_\parallel}$, and integrated over all $v_\perp$ must be positive. Taking into account the sign of $k_\parallel$ with the expression $\frac{k_\parallel}{|k_\parallel|}$, this will occur when regions of large positive $\frac{k_\parallel}{|k_\parallel|} \frac{\partial F}{\partial v_\parallel}$ exist along the integration path. Considering the m = +1 cyclotron term for the case when $k_\parallel$ is negative, the first term in Equation 4 is negative. Consequently, the m = +1 cyclotron resonance contribution to the growth rate

will be be positive when regions of large anisotropy, $\frac{\partial F}{\partial \alpha} > 0$, exist along the integration path.

Of the three electron distribution functions shown in Figure 2, only the distribution function measured on October 15, 1978, generates whistler mode waves via the m = 0 and the m = +1 resonances. This is because the convection speeds for the electron beams in the distribution functions measured on December 13, 1977, are large. Because the convection speeds are large, $\frac{\partial F}{\partial v_{\parallel}}$ is near zero at typical Landau resonance velocities and the Landau contribution to the growth rate is small. Consequently, the m = -1 cyclotron contribution to damping dominates any positive contribution to the growth rate due to the m = +1 cyclotron resonance. This is not the case for the electron distribution function measured on October 15, 1978, which has a smaller beam velocity. Because the beam velocity is small, the m = 0 Landau contribution to ω_i is large and positive.

The left column of Figure 5 presents a sample of the growth rates obtained using the October 15, 1978, electron distribution function. The results are given for one frequency, $\frac{\omega_r}{2\pi}$ = 80 Hz. At this time, $\frac{\omega_g}{2\pi}$ is about 110 Hz and $\frac{\omega_p}{2\pi}$ is about 20 kHz. The top left panel shows the m = 0 Landau resonance contribution to the ratio $\frac{\omega_i}{\omega_r}$ while the bottom left panel gives the m = +1 cyclotron resonance contribution to $\frac{\omega_i}{\omega_r}$. The m = -1 cyclotron resonance contribution to $\frac{\omega_i}{\omega_r}$ is negative and negligible for these wave normal angles and this frequency. The right column of Figure 5 depicts the Landau resonance velocity and the m = +1 cyclotron resonance velocity as a function of wave normal angle for $\frac{\omega_r}{2\pi}$ = 80 Hz.

From Figure 5 it is observed that the Landau contribution to ω_i is a maximum at an intermediate wave normal angle and decreases to zero at 0° and θ_{Res} ($\theta_{Res} \approx 43°$ here). The contribution is positive over a wide range of wave normal angles because the Landau resonance velocity lies in a region of positive $\frac{k_\parallel}{|k_\parallel|} \frac{\partial F}{\partial v_\parallel}$ over a wide range of wave normal angles. The Landau growth rate goes to zero at 0° because the whistler mode wave is purely transverse at that angle and goes to zero at θ_{Res} because the index of refraction for the whistler mode becomes very large near θ_{Res}, thereby moving the resonance velocity out of the region of large positive $\frac{k_\parallel}{|k_\parallel|} \frac{\partial F}{\partial v_\parallel}$.

The m = +1 cyclotron resonance contribution to ω_i is positive for wave normal angles between about 10° and 42°. The m = +1 contribution falls to zero as the wave normal angle approaches 0° because L_{+1} in Equation 1 is identically zero at 0°. This corresponds to the fact that a parallel propagating whistler mode wave is right-hand polarized with respect to the magnetic field, whereas the anomalous m = +1 resonance requires a left-hand polarization component for a resonant interaction to occur. The m = +1 contribution is zero for wave normal angles greater than about 42° because the m = +1 cyclotron resonance velocity does not lie in a region of sufficiently positive $\frac{\partial F}{\partial \alpha}$ for wave normal angles greater than 42°.

In Figure 6, the range of unstable resonance velocities for the m = 0 and the m = +1 resonances, as obtained from Figure 5, is overlayed on a contour plot of the October 15, 1978, electron distribution function. The Landau resonance velocity lies in a region of positive

$\frac{k_\parallel}{|k_\parallel|} \frac{\partial F}{\partial v_\parallel}$ while the m = +1 cyclotron resonance velocity lies in regions of large anisotropy, $\frac{\partial F}{\partial \alpha} > 0$.

Figures 7 and 8 summarize the unstable frequencies and wave normal angles for the electron distribution functions shown in Figure 2. Figure 7 depicts the waves that are generated by the m = 0 and +1 resonances for the October 15, 1978, velocity distribution. The unstable region is indicated by the shading. These waves have $k_\parallel < 0$, corresponding to wave vectors directed toward the magnetosheath. The unstable frequencies and wave normal angles for generation via the m = -1 resonance are shown in Figure 8. In the bottom panel, the results for the October 15, 1978, distribution are shown while the top panels correspond to the two December 13, 1977, distributions. These whistler mode waves are all generated by the m = -1 cyclotron resonance term and have $k_\parallel > 0$.

It is desirable to identify the growth rates that are large enough to produce a rapid increase in the intensity of whistler mode noise at Earth's bow shock. To do so, the critical growth rate, ω_c, required to produce large growth over a small distance is calculated. For simplicity, the critical growth rate is defined to be the growth rate necessary for an order of magnitude increase in the amplitudes of the wave electric and magnetic fields over a distance of 100 km. An order of magnitude increase in the intensity of whistler mode noise at Earth's bow shock is consistent with plasma wave observations (e.g., see Rodriguez and Gurnett [1975]). The spatial length over which the growth occurs, 100 km, is in agreement with bow shock scale lengths obtained by Russell [1979].

To calculate the critical growth rate, the effect of the solar wind flow on the propagation of a whistler mode wave packet must be taken into account. This is because the solar wind speed is often comparable to the whistler mode group speed. Because only a rough estimate of the critical growth rate is desired, two extreme situations are considered: wave packets with group velocities in the direction of the solar wind flow and wave packets with group velocities in the opposite direction of the solar wind flow. The critical growth rates for these two cases are given by

$$\omega_c(k_\parallel<0) = \frac{\ell n\ 10}{L}\ (v_g + v_{sw}) \tag{5}$$

and

$$\omega_c(k_\parallel>0) = \frac{\ell n\ 10}{L}\ (v_g - v_{sw}) \quad . \tag{6}$$

In these equations, v_g is the whistler mode group speed, v_{sw} is the solar wind speed, and L = 100 km is the characteristic scale length of the transition region. The group speed is calculated using

$$v_g = \frac{2c\ \omega_r^{1/2}\ (\omega_g \cos\ \theta - \omega_r)^{3/2}}{\omega_p\ \omega_g \cos\ \theta} \tag{7}$$

where c is the speed of light and θ is the wave normal angle. The solar wind speed is taken to have the constant value 400 km/s.

Equations 5 and 6 are used to calculate the critical growth rate for waves with wave vectors directed toward the magnetosheath, $k_{\parallel} < 0$, and for waves with wave vectors directed toward the solar wind, $k_{\parallel} > 0$. The results obtained are summarized in Figures 7 and 8. The region contained inside the dashed line in Figure 7 defines the frequencies and wave normal angles that have a growth rate, ω_I, greater than the critical growth rate, $\omega_c(k_{\parallel} < 0)$. For wave vectors directed toward the magnetosheath, $k_{\parallel} < 0$, waves with frequencies between about 5 and 85 degrees and with intermediate wave normal angles have the largest growth rates. For wave vectors directed toward the solar wind, $k_{\parallel} > 0$, Figure 8 illustrates that nearly all of the growth rates for the velocity distributions measured on October 15, 1978, and at 1734:55.7 on December 13, 1977, are large. However, the distribution obtained at 1734:58.5 on December 13, 1977, does not contain enough free energy to produce growth rates larger than the critical growth rate. At this time it is not known whether or not this is a common feature of velocity distributions that are measured at large shock penetration lengths.

It should be noted that the calculated growth rates are sometimes so large that the condition $\omega_I/\omega_r << 1$ is not satisfied. When this condition is not met, the growth rate calculated using Equation 1 is not accurate. It is expected that a more exact calculation of the growth rate would yield a smaller positive value. While this difficulty does point out the fact that some of the growth rates presented in this paper are rough estimates, the signs of the calculated growth rates are accurate.

V. DISCUSSION

This study has shown that electron distribution functions measured using the fast plasma experiment on ISEE 2 within the transition region of Earth's bow shock are unstable to a large spectrum of whistler mode waves. The unstable whistler mode waves have plasma rest frame frequencies between about .1 and 100 Hz and have wave vector directions with respect to the magnetic field which range from 0° to the resonance cone angle. In general, the lower frequency (.1 to 10 Hz) waves have wavelengths between about 500 and 100 km, while the higher frequency waves (10 to 100 Hz) have wavelengths between about 100 and 20 km. The whistler mode waves are generated by either electromagnetic Landau resonance or electromagnetic cyclotron resonance or both. The free energy regions in the electron distribution functions are regions of positive $\frac{k_\parallel}{|k_\parallel|}\frac{\partial F}{\partial v_\parallel}$ and regions of $T_\perp > T_\parallel$ anisotropy, both attributable to the field-aligned electron beam. If it is assumed that a background continuum of whistler mode noise is available in the solar wind for amplification, as indicated by the measurements of Neubauer et al. [1977], the stability calculations indicate that many of the unstable frequencies and wave normal angles have growth rates large enough to give rise to large whistler mode intensities at Earth's bow shock.

To fully evaluate the growth of whistler mode noise in the bow shock, it is necessary to compute the growth integrated along typical ray paths through the shock. However, a detailed treatment of this

problem is difficult because the magnetic field geometry within the transition region of Earth's bow shock is complicated. To obtain a qualitative understanding of the subsequent propagation of the generated whistler mode waves, a simple model for the shock geometry is adopted. The model is that of a parallel shock with the upstream solar wind velocity in the opposite direction of the shock normal. The ramp in the magnetic field amplitude defines the shock transition region where the electron distribution functions shown in Figure 2 are present. The electron distribution function measured on October 15, 1978, represents the distribution function often observed near the upstream boundary of the magnetic ramp. The electron distribution functions measured on December 13, 1977, represent the distribution functions often observed within the magnetic ramp.

The waves depicted in Figure 7 are produced near the upstream boundary of the magnetic ramp by the $m = 0$ and the $m = +1$ resonances and have $k_{\parallel}$ in the downstream direction. Because the waves with frequencies between about 5 and 85 Hz have the largest growth rates, at the upstream shock boundary a rapid increase in whistler mode intensity over this frequency range is expected. For the parallel shock model the wave packets propagate downstream and are convected downstream by the solar wind flow. This is due to the fact that the group velocity of the whistler mode is confined to angles less than about 20° from the magnetic field [Helliwell, 1965]. As these wave packets move downstream, they will encounter distribution functions similar to those measured on December 13, 1977. Because the electron distribution functions measured on December 13, 1977, are stable to waves with $k_{\parallel} < 0$, the waves will be

damped as they move downstream. It is expected that most of these waves will not reach the magnetosheath as the damping rate can be large.

The waves depicted in Figure 8 are generated by the m = -1 cyclotron resonance and have $k_{\parallel}$ in the upstream direction. For the simple shock model adopted the solar wind will convect the wave packets downstream if the group speed is smaller than the solar wind speed, which has the typical value 400 km/s. For plasma parameters typical of the bow shock region and for the frequencies of interest in this study, the group speed of the whistler mode is smaller than 400 km/sec for wave normal angles near θ_{Res}. Consequently, in the simple shock model only the whistler mode waves with wave normal angles near the resonance cone angle are convected downstream by the solar wind flow. The remaining whistler mode waves either travel upstream against the solar wind flow or stand in the shock. It is possible that the standing whistlers so produced contribute to the overall shock structure because many of the standing whistlers have wavelengths equal to the shock thickness.

Because the electron distribution function measured on October 15, 1978, represents the typical distribution near the upstream shock boundary the growth rate calculations for this distribution predict which whistlers will travel into the solar wind. The calculations summarized in the bottom panel of Figure 8 suggest that low frequency ($\approx$ 7 - 30 Hz) waves travel into the upstream solar wind. A range in wave normal angles from 0° to near θ_{Res} is expected.

These predictions are summarized as follows:

1) Intense broadband whistler mode noise is generated by the m = 0, +1, and -1 resonances in the shock transition region.

2) The whistler mode noise in front of the magnetic ramp will be most prevalent at low (7 - 30 Hz) frequencies. These waves are generated by the normal, m = -1, cyclotron resonance, and have wave normal angles from 0° to near θ_{Res}.

3) At the upstream boundary of the magnetic ramp, whistler mode waves with frequencies between about .1 and 100 Hz are produced via the m = 0 and +1 resonances. The waves with frequencies between about 5 and 85 Hz have the largest growth rates. Because these waves are damped as they travel downstream, most of the waves are not expected to reach the magnetosheath.

It is desirable to compare the predictions of this study with observations of whistler mode waves near Earth's bow shock. However, because the predicted frequencies are with respect to the plasma rest frame, they are not the frequencies actually measured by a plasma wave receiver. The measured frequencies are Doppler-shifted by the relative motion of the satellite and the plasma. Simple calculations show that in most cases the measured frequency is expected to be between about one-half to two times the rest frame frequency. Because the Doppler effect at the shock is difficult to treat in detail, in this paper only a qualitative comparison of the predictions of the study and observations of whistler mode waves will be made.

In Figure 9, data obtained on December 13, 1977, by the plasma wave experiment and the magnetic field experiment on board ISEE 1 are shown. ISEE 1, as opposed to ISEE 2, data are shown because wave magnetic field measurements, which are most useful for detecting whistler mode noise, were only available from ISEE 1 for the event studied. The spatial

separation of the two satellites is small. By comparing the ISEE 1 and the ISEE 2 magnetic field profiles at these times, the temporal separation of the two data sets measured on December 13, 1977, is found to be about 15 seconds. For example, the time 1735:00.0 on ISEE 2 corresponds to 1735:15.0 on ISEE 1.

The top panel of Figure 9 shows the wave magnetic fields in ten channels covering the frequency range 5.6 Hz to 1 kHz and the time period 1730:00.0 to 1740:00.0 UT on December 13, 1977. The bottom panel depicts the magnetic field strength over the same time period. The magnetic ramp defining the shock transition region is clearly visible, with the upstream boundary at about 1735:05.0. At this time, the satellite enters the shock from the solar wind. It is assumed that the electron distribution function at the upstream boundary of the magnetic ramp is similar to the October 15, 1978, electron distribution function. Within the magnetic ramp at about 1735:20.0, the electron distribution functions are those measured by the ISEE 2 fast plasma experiment on December 13, 1977.

In Figure 9, whistler mode noise is visible in the bottom six frequency channels of the wave magnetic field data. As predicted by this study, the noise has largest intensity within the magnetic ramp. The frequency range over which the noise is observed, from about 5.6 to 100 Hz, is in good agreement with the results of this study. In the solar wind immediately upstream of the magnetic ramp, the noise is most intense at low frequencies, in agreement with prediction 2 above. This figure, which is typical of whistler mode observations at the bow shock, illustrates that the predictions of this study and the observations of whistler mode waves compare favorably.

ACKNOWLEDGEMENTS

The authors thank S. P. Gary at Los Alamos and M. W. Hodges at Iowa for their contributions to this study. We also thank C. T. Russell at UCLA for providing the ISEE magnetometer data.

This research was supported by NASA through Grants NGL-16-001-002 and NGL-16-001-043 from NASA Headquarters and Contract NAS5-26819 from Goddard Space Flight Center and by the Office of Naval Research through Contract N00014-76-C-0016.

TABLE 1

Parameters Which Specify the Electron Distribution Functions in Figure 2

DATE AND TIME (UT)	C_1 (Arbitrary Units)	C_2 (Arbitrary Units)	v_1 (km/s)	v_2 (km/s)	v_3 (km/s)	P	R	$T_\perp$ (°K)	$T_\parallel$ (°K)
10/15/78 1821:02.0	6.14×10^7	6.00×10^7	0.0	2600.0	1970.0	3.29	2.29	4.00×10^5	3.60×10^4
12/13/77 1734:55.7	2.10×10^7	1.20×10^7	0.0	3650.0	3255.0	3.43	2.43	2.70×10^5	2.00×10^4
12/13/77 1734:58.5	8.05×10^6	7.10×10^6	277.0	5250.0	5363.0	4.26	3.00	2.60×10^5	2.40×10^4

TABLE 2

Shock Parameters

DATE AND TIME (UT)	θ_{Bn} (Degrees)	Magnetic Local Time (Hours)	Radial Distance (R_E)	$\omega_p/2\pi$ (kHz)	$\omega_g/2\pi$ (Hz)
10/15/78 1821:02.0	35	12.6	14.3	20	110
12/13/77 1734:55.7	65	8.2	16.8	20	315
12/13/77 1735:00.0	65	8.2	16.8	20	315
12/13/77 1734:58.5	65	8.2	16.8	20	315

REFERENCES

Bame, S. J., J. R. Asbridge, H. E. Felthauser, J. P. Glore, G. Paschmann, P. Hemmerich, K. Lehmann, and H. Rosenbauer, ISEE-1 and ISEE-2 fast plasma experiment and the ISEE-1 solar wind experiment, IEEE Trans. Geosci. Electron., GE-16, 216, 1978.

Feldman, W. C., S. J. Bame, S. P. Gary, J. T. Gosling, D. McComas, M. F. Thomsen, G. Paschmann, N. Sckopke, M. M. Hoppe, and C. T. Russell, Electron heating within the Earth's bow shock, Phys. Rev. Lett., 49, 199, 1982.

Feldman, W. C., R. C. Anderson, S. J. Bame, S. P. Gary, J. T. Gosling, D. J. McComas, M. F. Thomsen, G. Paschmann, and M. M. Hoppe, Electron velocity distributions near the Earth's bow shock, J. Geophys. Res., 88, 96, 1983.

Formisano, V., The physics of the Earth's collisionless shock wave, J. de Physique, 38, C6-65, 1977.

Forslund, D. W., J. M. Kindel, and M. A. Stroscio, Current driven electromagnetic ion cyclotron instability, J. Plasma Phys., 21, 127, 1979.

Fredericks, R. W., C. F. Kennel, F. L. Scarf, G. M. Crook, and I. M. Green, Detection of electric-field turbulence in the earth's bow shock, Phys. Rev. Lett., 21, 1761, 1968.

Galeev, A. A., Collisionless shocks, in Physics of Solar Planetary Environments, Vol. 1, ed. by D. J. Willians, American Geophysics Union, 1976.

Greenstadt, E. W., and R. W. Fredericks, Shock systems in collisionless space plasmas, in Solar System Plasma Physics, Vol III, ed. by C. F. Kennel, L. J. Lanzerotti, and E. N. Parker, North-Holland Publishing Company, 1979.

Greenstadt, E. N., R. W. Fredericks, C. T. Russell, F. L. Scarf, R. R. Anderson, and D. A. Gurnett, Whistler mode wave propagation in the solar wind near the bow shock, J. Geophys. Res., 86, 4511, 1981.

Gurnett, D. A., F. L. Scarf, R. W. Fredericks, and E. J. Smith, The ISEE 1 and ISEE 2 plasma wave investigation, IEEE Trans. Geosci. Electron., GE-16, 225, 1978.

Helliwell, R. A., Whistlers and related ionospheric phenomena, Stanford University Press, Stanford, California, 1965.

Kennel, C. F., Low-frequency whistler mode, Phys. of Fluids, 9, 2190, 1966.

Kennel, C. F., and H. V. Wong, Resonant particle instabilities in a uniform magnetic field, J. Plasma Physics, 1, 75, 1967.

Leimohn, H. B., and F. L. Scarf, Whistler attenuation by electrons with an $E^{-2.5}$ distribution, J. Geophys. Res., 67, 4163, 1962.

Neubauer, F. M., H. J. Beinroth, H. Barnstorf, and G. Dehmel, Initial results from the Helios-1 search coil magnetometer experiment, J. Geophys. Res., 42, 599, 1977.

Rodriguez, P., and D. A. Gurnett, Electrostatic and electromagnetic turbulence associated with the Earth's bow shock, J. Geophys. Res., 80, 19, 1975.

Russell, C. T., The ISEE-1 and -2 fluxgate magnetometers, IEEE Trans. Geosci. Electron., GE-16, 239, 1978.

Russell, C. T., and E. W. Greenstadt, Initial ISEE magnetometer results: Shock observations, Space Sci. Rev., 23, 3, 1979.

Tidman, D. A., and N. Krall, Shock Waves in Collisionless Plasmas, John Wiley-Interscience, New York, 1971.

FIGURE CAPTIONS

Figure 1 This figure, reproduced from Feldman et al. [1982], shows parallel slices of electron distribution function data measured by the ISEE 2 fast plasma experiment. As the satellite moves from the solar wind into the magnetosheath, field-aligned electron beams are observed.

Figure 2 This figure depicts contour plots of the logarithm of the analytic fits to the electron distribution function data analyzed in this study. These distribution functions were measured within the transition region of Earth's bow shock. A modified Lorentzian models the flat-topped component of the electron distribution and a convected Maxwellian with a $T_{\perp} > T_{\parallel}$ anisotropy models the field-aligned electron beam.

Figure 3 The left column of this figure presents a sample of the growth rates obtained for the electron distribution function measured on December 13, 1977, at 1735:55.7. Plotted is the ratio of the total growth rate to real frequency. These waves are

generated by the m = -1 cyclotron resonance and have $k_{\parallel} > 0$. The right column of this figure depicts the m = -1 cyclotron resonance velocity as a function of wave normal angle for the two frequencies of interest.

Figure 4 In this figure, the range in the m = -1 cyclotron resonance velocity corresponding to instability for $\omega_r/2\pi$ = 110 Hz, as obtained from Figure 2, is overlayed on a contour plot of the electron distribution function measured on December 13, 1977, at 1734:55.7. The m = -1 cyclotron resonance velocities lie in regions of large anisotropy, $\frac{\partial F}{\partial \alpha} < 0$.

Figure 5 The left column of this figure presents a sample of the growth rates obtained for the electron distribution function measured on October 15, 1978, and for the frequency $\omega_r/2\pi$ = 80 Hz. The unstable waves have $k_{\parallel} < 0$, corresponding to wave vectors directed toward the magnetosheath. The top left panel shows the m = 0 Landau contribution to the growth rate while the bottom left panel shows the m = +1 cyclotron contribution to the growth rate. For this frequency and these wave normal angles the m = -1 cyclotron contribution to ω_i/ω_r are negative and negligible. The right column depicts both the m = 0 Landau resonance

velocity and the m = +1 cyclotron resonance velocity as a function of the wave normal angle.

Figure 6 — In this figure, the range in the m = 0 Landau and the m = +1 cyclotron resonance velocities corresponding to instability for the case $\omega_r/2\pi$ = 80 Hz, as obtained from Figure 4, is overlayed on a contour plot of the electron distribution function measured on October 15, 1978. The m = 0 Landau resonance velocities lie in regions of positive $\frac{k_\parallel}{|k_\parallel|}\frac{\partial F}{\partial v_\parallel}$ while the m = +1 cyclotron resonance velocities lie in a region of large anisotropy, $\frac{\partial F}{\partial \alpha} > 0$.

Figure 7 — This figure depicts the unstable frequencies and wave normal angles that are generated by the m = 0 and +1 resonances for the electron distribution function measured on October 15, 1978. The waves have $k_\parallel < 0$, corresponding to wave vectors directed toward the magnetosheath. The largest growth rates lie in the shaded region bounded by the dashed line.

Figure 8 — This figure depicts the unstable frequencies and wave normal angles that are generated by the m = -1 cyclotron resonance for the electron distribution functions shown in Figure 2. All of the waves and have $k_\parallel > 0$, corresponding to wave vectors directed toward the

solar wind. The growth rates for the distribution measured at 1734:58.5 on December 13, 1977, are smaller than the critical growth rate.

Figure 9 This figure depicts data obtained with the ISEE-1 plasma wave experiment and the magnetic field experiment. The top panel shows the wave magnetic fields for six frequency channels. The bottom panel illustrates the magnetometer data. The magnetic ramp at the shock is clearly visible. The characteristics of the whistler mode noise at the shock are in good agreement with the predictions of this study.

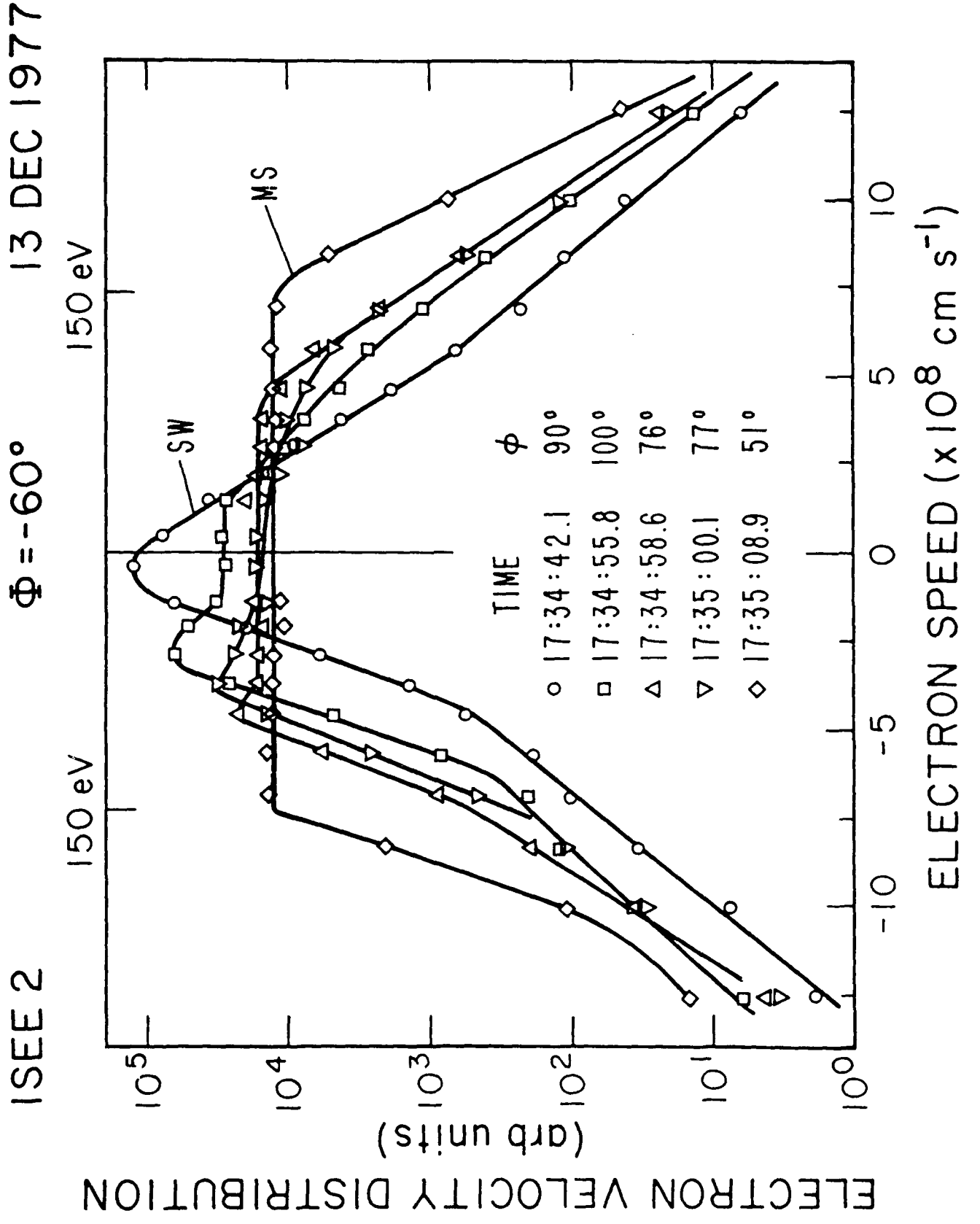
ISEE 2
Φ=-60°
13 DEC 1977
150 eV
150 eV
SW
MS
TIME
φ
○ 17:34:42.1 90°
□ 17:34:55.8 100°
△ 17:34:58.6 76°
▽ 17:35:00.1 77°
◇ 17:35:08.9 51°
ELECTRON VELOCITY DISTRIBUTION
(arb units)
ELECTRON SPEED (x10⁸ cm s⁻¹)

Figure 1

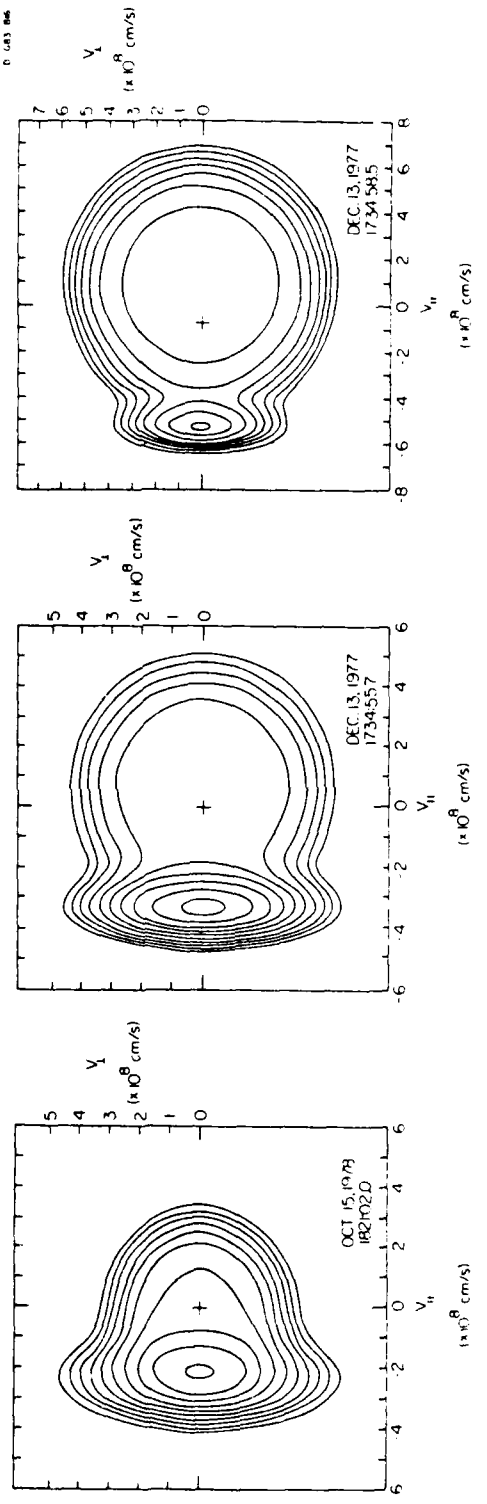
OCT. 15, 1978
182102.0
DEC. 13, 1977
173455.7
DEC. 13, 1977
173458.5
$V_\perp$
$V_\parallel$
$(\times 10^8$ cm/s)

Figure 2

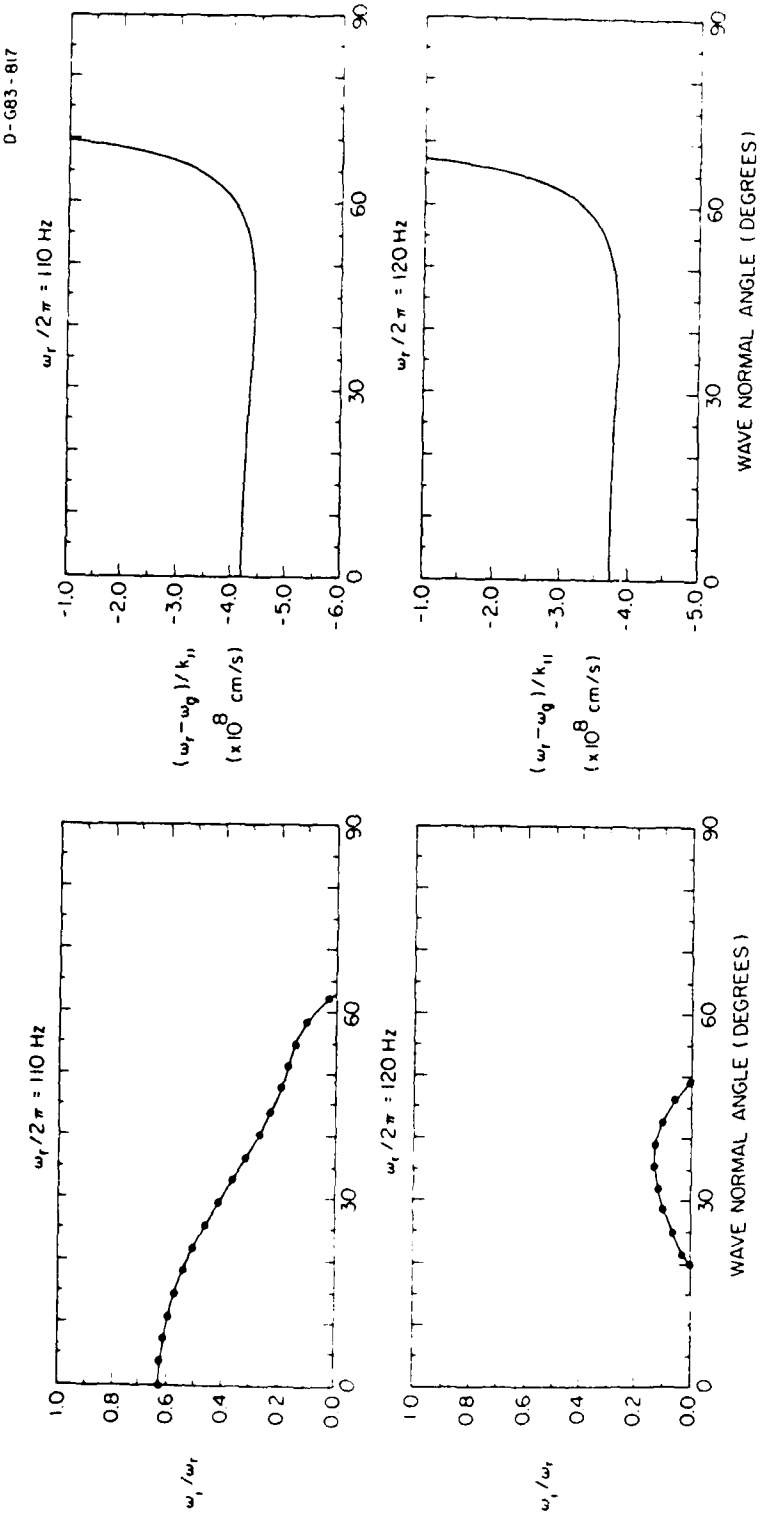
D-G83-817
$\omega_r/2\pi$ = 110 Hz
$\omega_r/2\pi$ = 120 Hz
$(\omega_r-\omega_g)/k_{||}$
($\times 10^8$ cm/s)
ω_i/ω_r
WAVE NORMAL ANGLE (DEGREES)

Figure 3

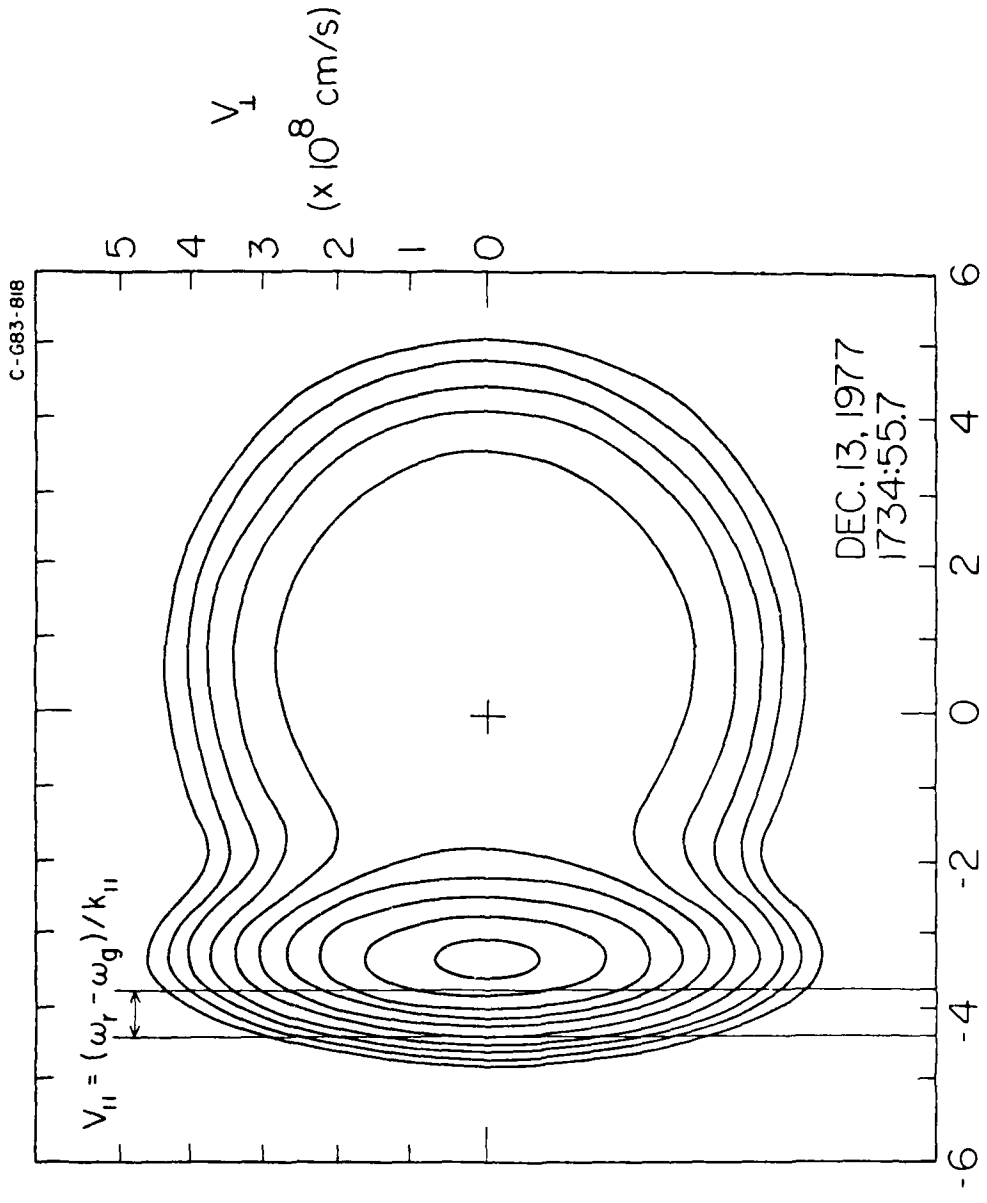
C-683-818
$V_\perp$
(x 10^8 cm/s)
5
4
3
2
1
0
DEC. 13, 1977
1734:55.7
$V_{11} = (\omega_r - \omega_g)/k_{11}$
6
4
2
0
-2
-4
-6
V_{11}
(x 10^8 cm/s)

Figure 4

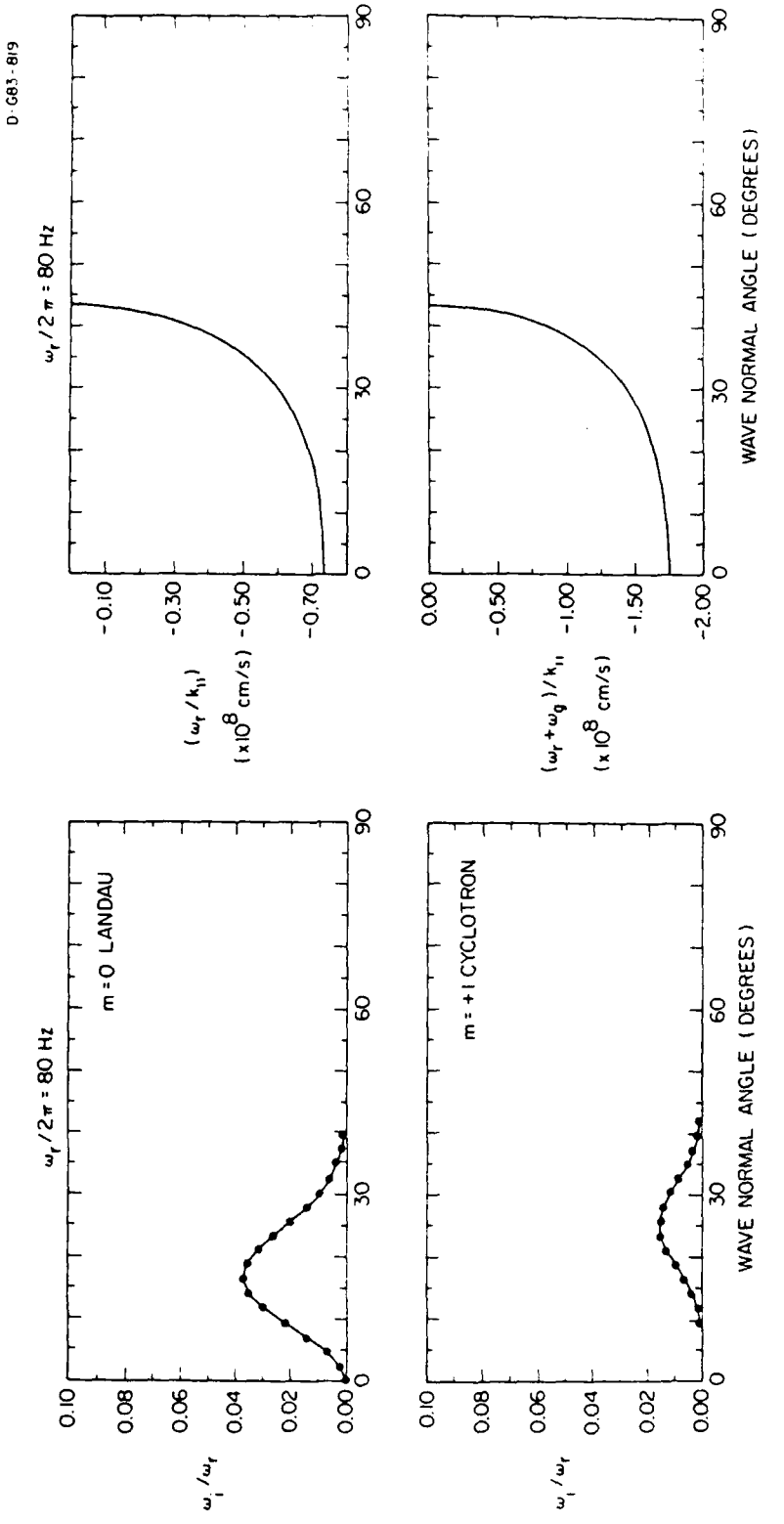
D-GB3-819
$\omega_r/2\pi$ = 80 Hz
$(\omega_r/k_{||})$
$(\times 10^8$ cm/s)
-0.10
-0.30
-0.50
-0.70
0
30
60
90
$(\omega_r+\omega_g)/k_{||}$
$(\times 10^8$ cm/s)
0.00
-0.50
-1.00
-1.50
-2.00
WAVE NORMAL ANGLE (DEGREES)
$\omega_r/2\pi$ = 80 Hz
m = 0 LANDAU
m = +1 CYCLOTRON
ω_i/ω_r
0.10
0.08
0.06
0.04
0.02
0.00
WAVE NORMAL ANGLE (DEGREES)

Figure 5

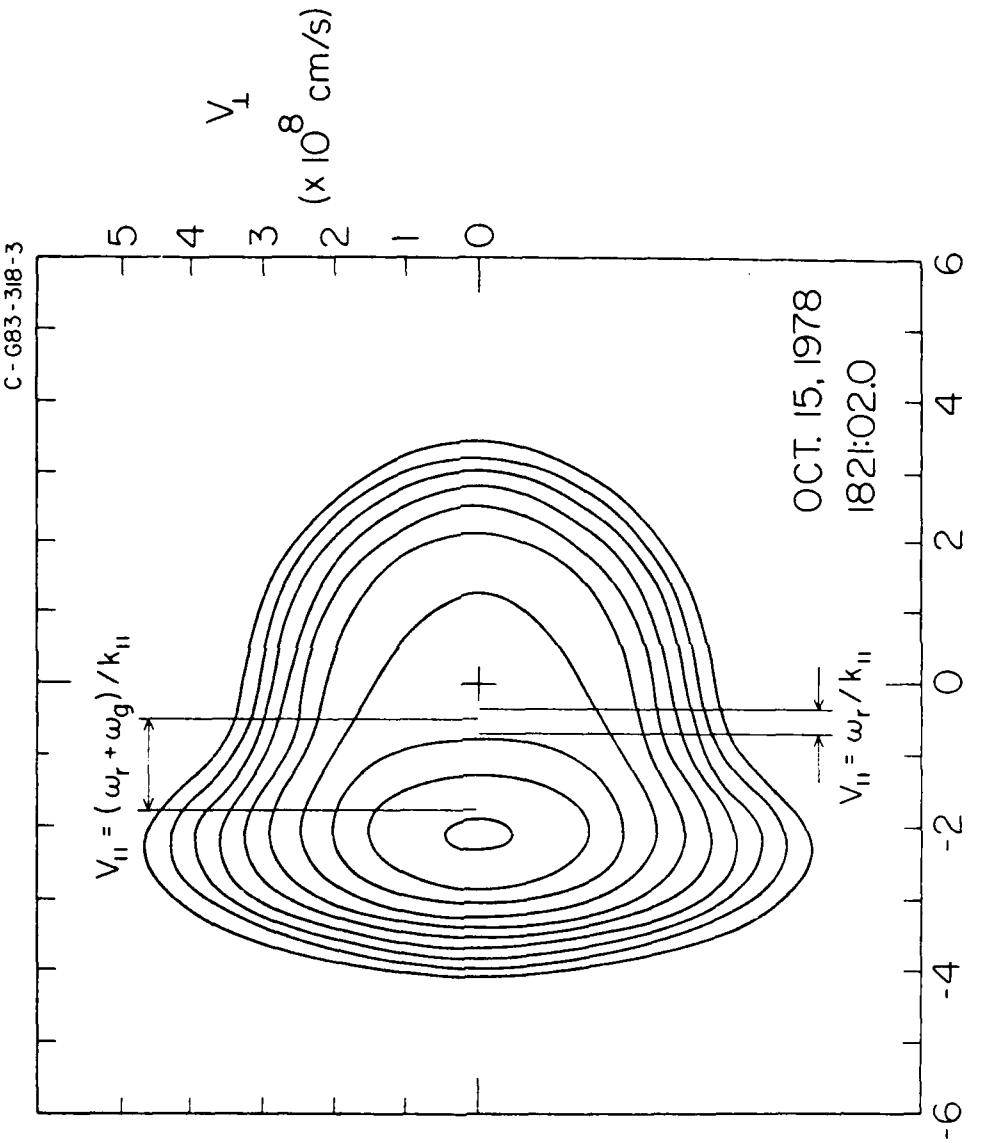
C-G83-318-3
$V_\perp$
(x 10^8 cm/s)
5
4
3
2
1
0
OCT. 15, 1978
1821:02.0
$V_{11} = (\omega_r + \omega_g)/k_{11}$
$V_{11} = \omega_r/k_{11}$
6
4
2
0
-2
-4
-6
V_{11}
(x 10^8 cm/s)

Figure 6

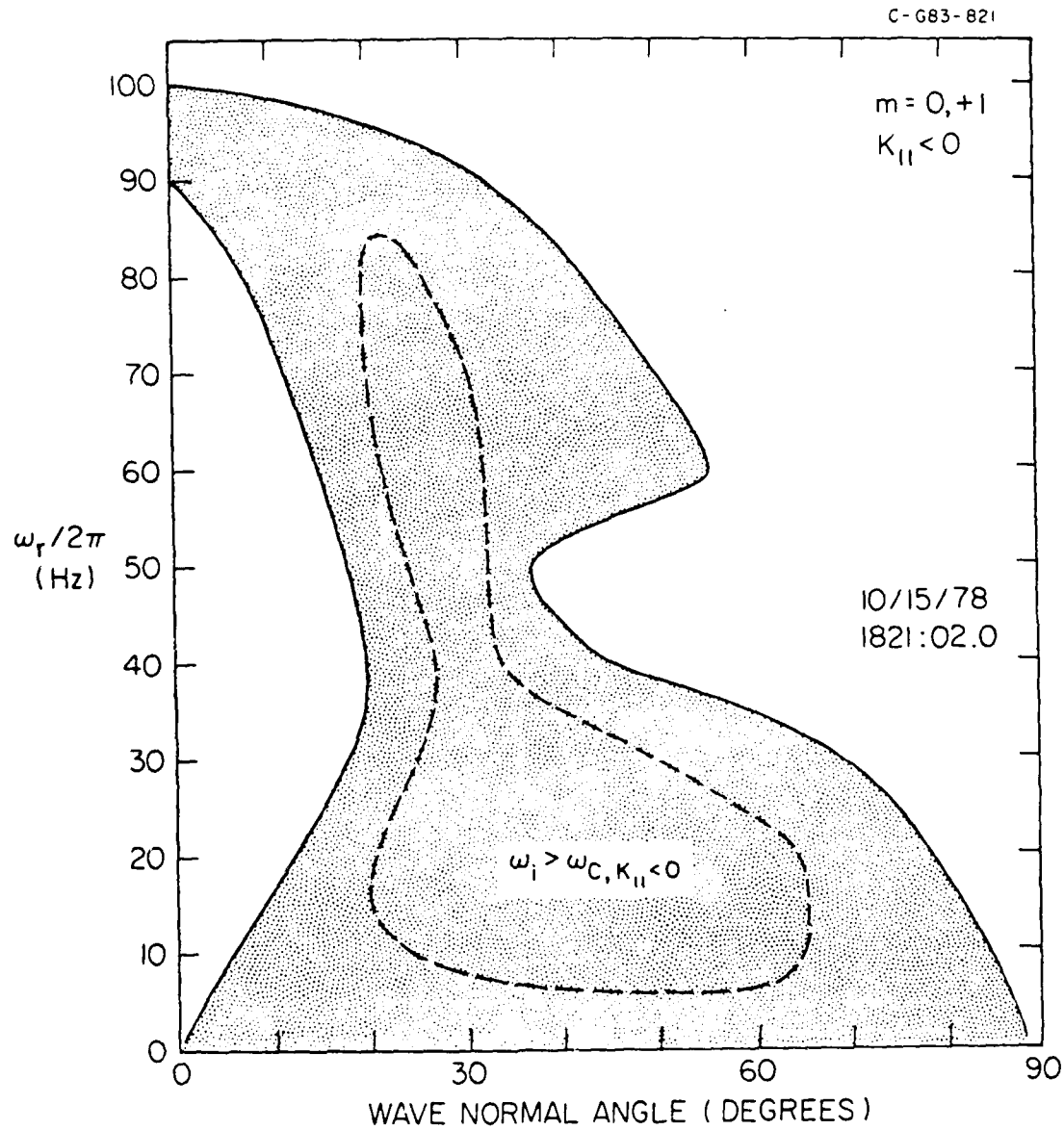
C-G83-821
m = 0, +1
$K_{11} < 0$
10/15/78
1821:02.0
$\omega_i > \omega_c, K_{11} < 0$
$\omega_r/2\pi$
(Hz)
100
90
80
70
60
50
40
30
20
10
0
0
30
60
90
WAVE NORMAL ANGLE (DEGREES)

Figure 7

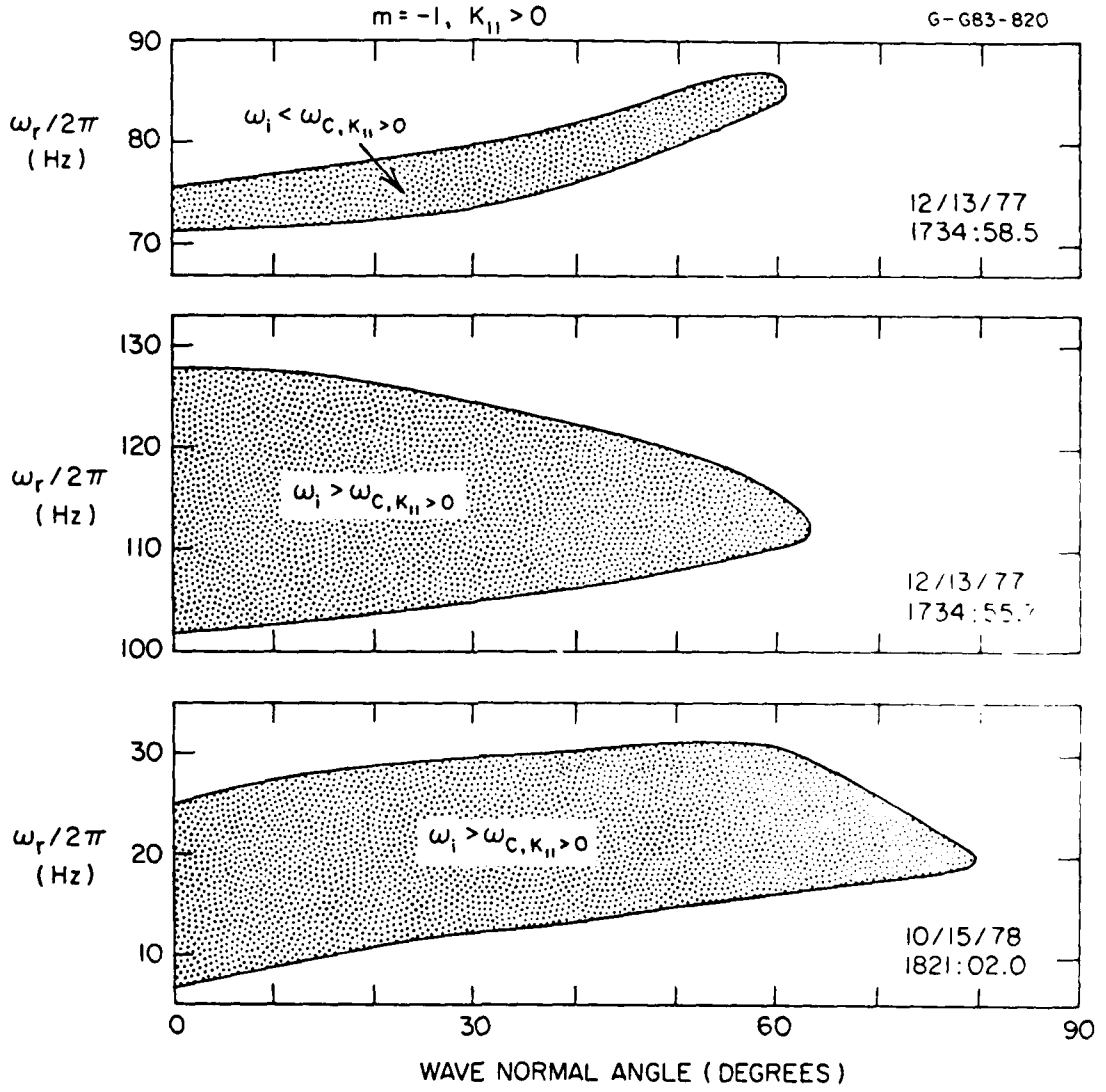
m = -1, $K_{\parallel} > 0$
G-G83-820
$\omega_r/2\pi$ (Hz)
90
80
70
$\omega_i < \omega_{C,K_{\parallel}>0}$
12/13/77
1734:58.5
130
120
110
100
$\omega_i > \omega_{C,K_{\parallel}>0}$
12/13/77
1734:55.7
30
20
10
$\omega_i > \omega_{C,K_{\parallel}>0}$
10/15/78
1821:02.0
0
30
60
90
WAVE NORMAL ANGLE (DEGREES)

Figure 8

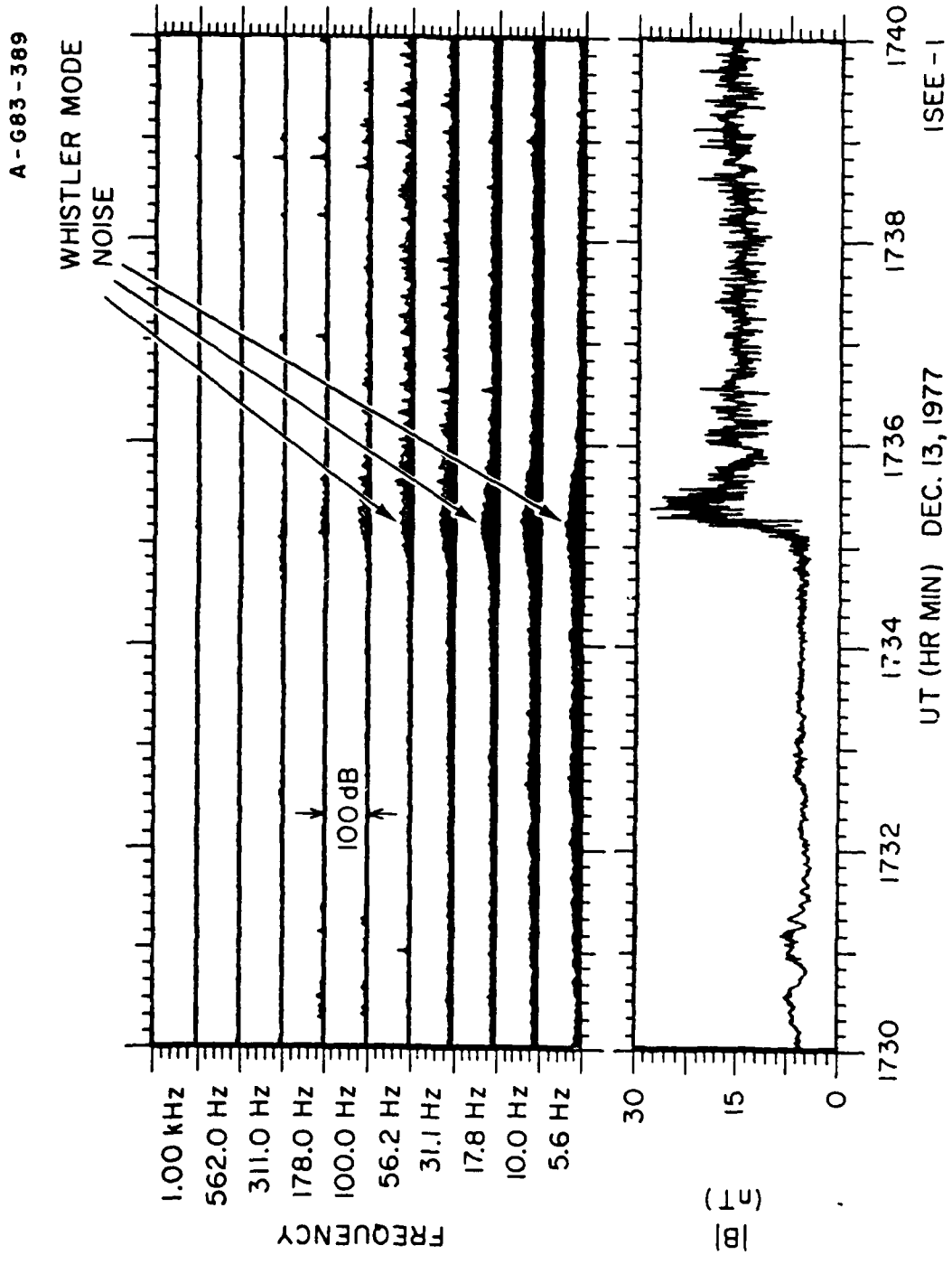
A-683-389
WHISTLER MODE
NOISE
100 dB
1.00 kHz
562.0 Hz
311.0 Hz
178.0 Hz
100.0 Hz
56.2 Hz
31.1 Hz
17.8 Hz
10.0 Hz
5.6 Hz
FREQUENCY
|B| (nT)
30
15
0
1730
1732
1734
1736
1738
1740
UT (HR MIN) DEC. 13, 1977
ISEE-1

Figure 9

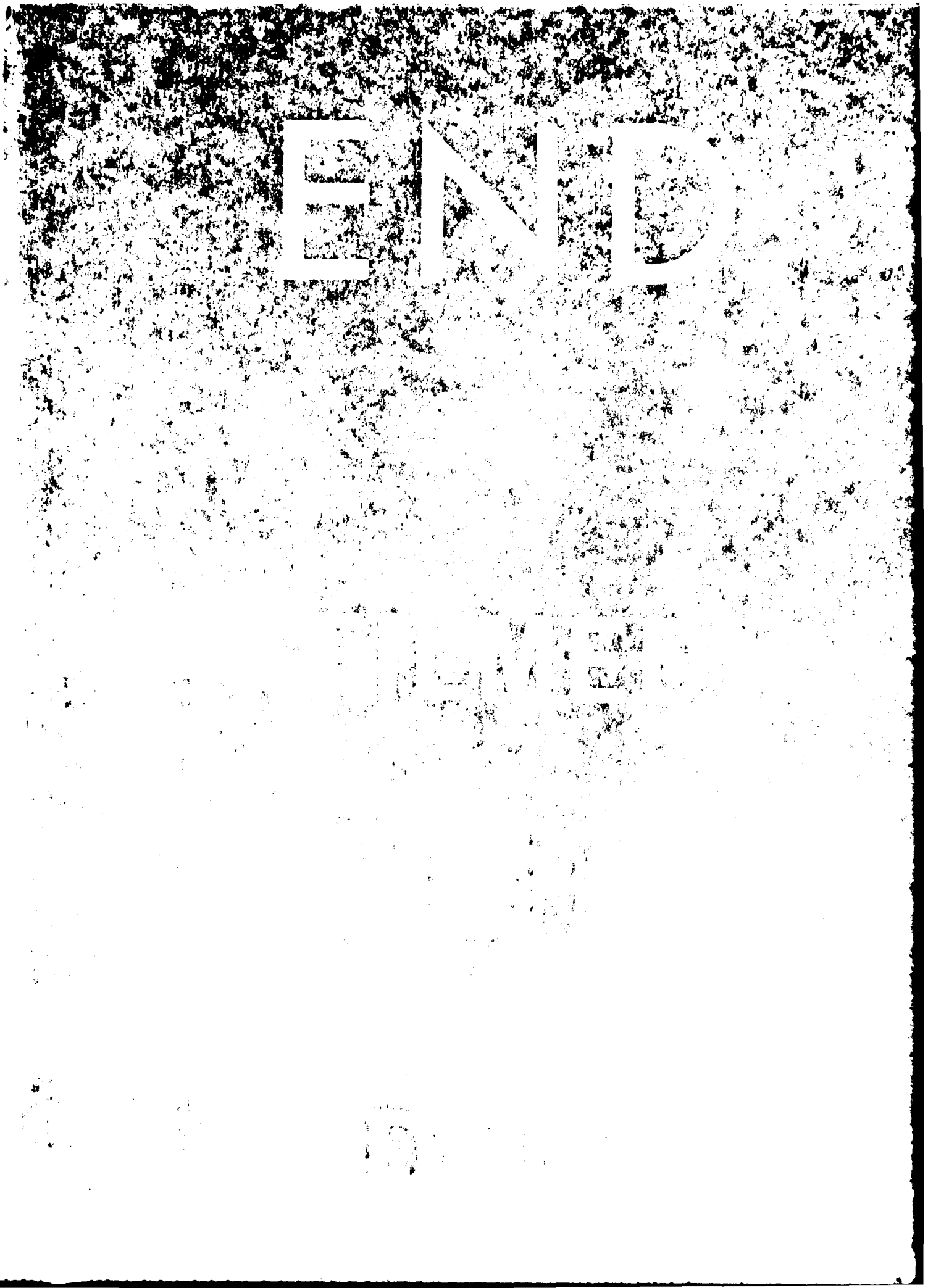
END